

## Autonomous Underwater Vehicle Measurements of Surface Wave Decay and Directional Spectra in the Marginal Sea Ice Zone\*

DANIEL R. HAYES<sup>+</sup> AND ADRIAN JENKINS

*British Antarctic Survey, Natural Environment Research Council, Cambridge, United Kingdom*

STEPHEN MCPHAIL

*National Oceanography Centre, Southampton, University of Southampton, and Natural Environment Research Council, Southampton, United Kingdom*

(Manuscript received 7 September 2005, in final form 8 May 2006)

### ABSTRACT

In March 2003 several autonomous underwater vehicle (AUV) missions were carried out under sea ice in the western Bellingshausen Sea. Data from the upward-looking acoustic Doppler current profiler (ADCP) on the "Autosub" AUV indicate a strongly oscillating horizontal velocity of the ice due to ocean swell. Swell period, height, direction, and directional spread have been computed every 800 m from the ice edge to 10 km inward for three missions. Exponential, period-dependent attenuation of waves propagating through sea ice was observed. Mean period increased with distance from the ice edge. The wave field refracted during propagation. The directional wave spread does not seem to relate to distance from the ice edge, although higher frequencies tended to be more spread. If suitably deployed, an ordinary ADCP may be used with this technique to study both scalar and directional properties of waves in open or ice-covered water.

### 1. Introduction

The measurement of scalar and directional wave properties is common in the open and coastal ocean. Buoys are most commonly used because, in addition to measuring wave height from vertical platform acceleration, they can also measure directional properties of waves through pitch and roll sensors (Longuet-Higgins

et al. 1963). It is also possible to measure wave properties from submerged sensors: usually pressure along an array or pressure and horizontal current velocity at a point are measured in the surface wave layer. Recently developed techniques to measure surface wave properties from acoustic Doppler current profilers (ADCPs) yield results that compare well with those obtained from pressure gauge arrays (Terray et al. 1997, 1999), but they require sophisticated algorithms and/or expensive equipment upgrades. The techniques described here can be applied to data collected with off-the-shelf ADCPs in an upward-looking configuration. In this study, the ADCP was mounted on an autonomous underwater vehicle (AUV). The measurement of directional spectra from submerged vehicles was first suggested by Munk in Macovsky and Mechlin (1963). The first wave measurements from a submerged vehicle in the open sea were made by De Leonibus (1963) and under sea ice by Wadhams (1978), both using submarine platforms. AUV wave observations (Earle et al. 2002; Brumley et al. 2003) hold advantages over point measurements and submarines. The mobility and spatial sampling possible with AUVs aid opera-

---

\* Based on "Surface Wave Decay and Directional Spectra in the Marginal Sea Ice Zone Measured by an Autonomous Underwater Vehicle," by D. Hayes, A. Jenkins, and S. McPhail, which appeared in *Proceedings of the IEEE/OES/CMTC Eighth Working Conference on Current Measurement Technology*, J. R. White and S. Anderson, Eds., The Printing House, © 2005 IEEE.

---

<sup>+</sup> Current affiliation: Oceanography Centre, University of Cyprus, Nicosia, Cyprus.

---

*Corresponding author address:* Daniel Hayes, Oceanography Centre, University of Cyprus, P.O. Box 20537, 1678 Nicosia, Cyprus.  
E-mail: dhayes@ucy.ac.cy

tions and management in coastal zones, open ocean, and ice-covered regions, including research, monitoring, commercial, and defense-related activities. While the technique of Earle et al. (2002) does not require an upward-looking ADCP, it requires the vehicle to be near the ocean surface. Using an ADCP, wave motion can be observed from an AUV in deep water, where the AUV is below the depth of influence of the waves. For some studies, such as the present one under sea ice, instruments must be operated at these depths for safety or other reasons.

Understanding waves in the marginal ice zone (MIZ) could be important in parameterizing their effect on ice–ocean–atmosphere interaction. For example, Wadhams (1986) makes a rough estimate of the basal melting of ice floes due to the wave-induced, oscillating horizontal current. A deeper understanding of the propagation of waves through sea ice may shed more light on such situations where ice–ocean turbulence is enhanced by waves, thus enhancing ice–ocean exchanges and potentially influencing the properties of the ice thickness distribution. The aggregate response of marginal ice zones to wave action is also of interest with regard to the possible effect on floe size distribution. Thus, there may be a benefit to including wave effects in ice–ocean numerical models. By understanding wave propagation in sea ice, it may be possible to develop algorithms to deduce some area-averaged property such as ice thickness based on observed propagation (Squire et al. 1995). It should be noted that thickness has been successfully estimated for pancake ice fields based on the observed wave dispersion (Wadhams et al. 2004).

MIZ studies often use buoys, heave-tilt sensors, and/or synthetic aperture radar (SAR). Naturally, the properties of waves in sea ice are significantly different from those of waves in the open ocean. The main result is that, in nearly all cases observed, surface waves have been attenuated exponentially with distance into the ice pack (Wadhams 1973, 1975, 1978). [Accumulation of wave energy deep in the ice pack has also been observed and modeled for the case of waves propagating in a continuous ice sheet (Liu and Mollo-Christensen 1988), but such cases will not be considered here.] Wadhams et al. (1988) established that in the MIZ attenuation increases as period decreases, until roughly 8–10 s, where the attenuation decreases again; this is called the “rollover” effect. The primary mechanism of attenuation in the MIZ is wave scattering by ice floes. Several scattering models have successfully predicted attenuation rates, and the most sophisticated also take into account the flexing of individual floes and irrecov-

erable damping due to turbulence, collisions, abrasions, and inelastic bending (Liu et al. 1991; Meylan et al. 1997).

Aside from the present work, there are few studies of how the directional properties of waves are affected by ice cover. One promising technique of collecting directional information is SAR. Larouche and Cariou (1992) used SAR to observe the spatial properties of a wave field in sea ice and suggested that inhomogeneities in the ice field (concentration or floe size) and/or current shear led to refraction of the wave field. SAR has also been used to examine waves propagating in pancake ice fields (Wadhams et al. 2002) and to estimate pancake ice thickness (Wadhams et al. 2004). Wadhams et al. (1986) used a combination of wave buoys and heave-tilt sensors to conclude that propagation through sea ice increased wave spread. Meylan et al. (1997) have made serious attempts at reproducing these few observations with a sophisticated model, with promising results. However, the model assumes a homogeneous ice field, so refraction is not predicted. It does, however, predict an increase in wave spread for waves propagating through the MIZ, especially for high frequencies.

In this paper the first use of an AUV to measure directional and scalar wave properties during surface wave propagation through sea ice is discussed. Observations of the spatial evolution of wave spectra with the preceding field and modeling studies will be compared. Both scalar and directional spectra will be computed. Like SAR, AUVs have advantages over accelerometer packages (on buoys or ice floes): they sample all surface types, not just open water or sufficiently large floes; they sample at high spatial resolution; and they sample a large portion of the MIZ over short time scales, over which the wave field is approximately steady. Last, AUVs are remote platforms, so when deployed appropriately they are not affected by wave motion. First the data collection is described, and then the calculation of wave properties and the results and implications are discussed.

## 2. Experiment description

From 22 to 25 March 2003 the Autosub AUV completed four missions under sea ice near Thurston Island, west of the Antarctic Peninsula (Fig. 1). Autosub is a 6.8-m long, 1-m diameter, battery-powered vehicle that executes preprogrammed courses at a speed of about  $1.6 \text{ m s}^{-1}$  up to a maximum range of 400 km. It carries several scientific instruments. Here only the upward-looking ADCP data will be discussed. Other observations include conductivity, temperature, and depth; vehicle pitch, yaw, and roll; and velocities from a

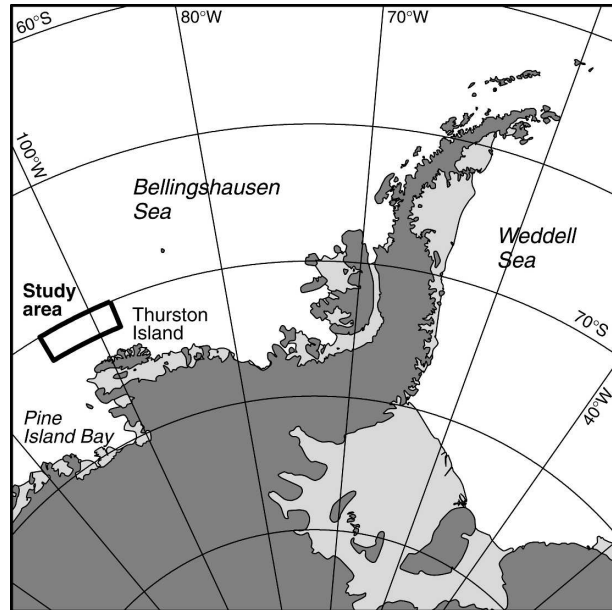


FIG. 1. Antarctic Peninsula with key place names. The study area is north of Thurston Island.

downward-looking ADCP. A detailed description of the Autosub is presented by Millard et al. (1998).

The upward-looking ADCP (a 300-kHz RDI Workhorse) was mounted in the aft section of the Autosub, covered by a 3-mm-thick polyethylene acoustic window. The four beams are in a Janus configuration, each with an angle of  $30^\circ$  to the vertical axis of the Autosub frame. Every second the ADCP alternately emits one profile ping or one surface ping. From the return of the profile ping, water velocity relative to the sub in fifteen 8-m-thick bins above Autosub is calculated. The surface track ping yields the range to the surface and the relative velocity of that surface. Surface returns were recorded from an instrument depth of up to about 200 m beneath sea ice, while in open water the surface echo, even from 90 m, was too weak to detect. This allowed ice edge detection (verified by shipboard observations).

In this experiment, the Autosub position was calculated in real time by integrating the relative velocity measurement from the nearest bin of the downward-looking ADCP (“water track” mode). The water was too deep for Autosub to navigate by tracking the ocean floor with the downward-looking ADCP, which has a maximum range of 500 m. In water track mode, the Autosub’s navigation frame of reference is the water rather than the seabed; hence for some missions a mean current caused the sub to drift from the mission plan. In postprocessing, therefore, Autosub GPS surface location fixes were used to calculate absolute AUV velocity (assuming a constant drift velocity between GPS fixes).

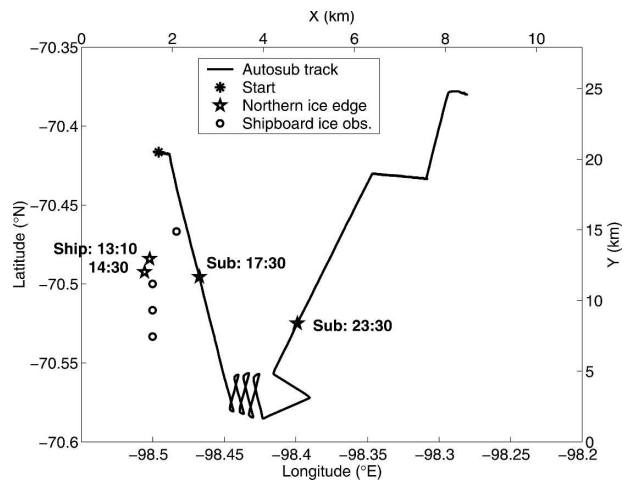


FIG. 2. Position of Autosub during mission 324 on 25 Mar 2003. The asterisk indicates the starting location of the mission. The stars indicate the observed locations of the northern ice edge. Those on the vehicle track were obtained from upward-looking ADCP data; the other two were observed from the *James Clark Ross* (*JCR*). Visual ice observations were made from the *JCR* at the locations indicated by circles. See the text for details.

All ADCP velocity measurements are then converted to absolute velocity in geographic coordinates.

The Autosub was deployed and recovered from the RRS *James Clark Ross* as part of Cruise JR84. Mission 324 on 25 March sampled an area of roughly  $10 \text{ km}^2$  of sea ice and traversed the ice edge twice: once upon entering the sea ice from the open ocean and once upon exiting (Fig. 2). Autosub was programmed to run a “lawnmower” pattern at 90-m depth, but this was distorted by the mean eastward ocean current at 90 m. The ice edge position was measured during the mission by the upward-looking ADCP as well as during predeployment shipboard observations (Fig. 2). Ice properties were recorded at four locations from the ship several kilometers into the ice. The three stations south of the ice edge reported 100% ice coverage: 20% brash and 80% multiyear or first-year ice of thickness 1.5–2 m. Floe diameter was less than 20 m. Outside the ice edge, at the northernmost ice observation station, only 60% coverage was observed, and this consisted of pancake and frazil ice. The ice edge was observed to lie approximately east–west. In this paper, the ice edge is defined as the point where ice type, thickness, and concentration all changed sharply from loose pancake and frazil to more compact first-year and multiyear floes. Winds were observed from the ship and were primarily from the northeast at  $15\text{--}20 \text{ m s}^{-1}$ . Swell of 9–10-s period was observed in ship roll and heave throughout the Autosub mission.

For mission 323 on 24 March, Autosub was deployed

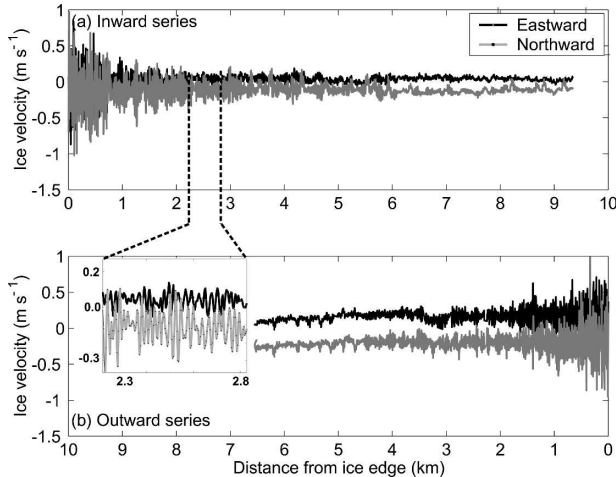


FIG. 3. Ice velocity from Autosub mission 324. The upward-looking ADCP measured the surface track velocity (a) upon entering the ice pack at 90 m and (b) exiting the ice pack at 90 m. The magnified inset view shows a typical segment analyzed here. Note the strong periodicity in both components as well as mean current toward the southeast.

at the ice edge, dove to 90 m, and entered the ice pack. It followed a lawnmower pattern before exiting the ice pack at 200 m. Ice coverage was 100%: 60% consisted of first-year ice floes less than 20-m diameter and 0.5 to 0.75 m thick, and 40% consisted of brash 50 cm thick. Winds were from the northeast at  $10\text{--}15\text{ m s}^{-1}$ . Spectra of ship roll and heave indicate swell of period 9–13 s. Mission 322 on 23 March was a one-way trip from inside the ice pack to a point north of the ice edge at 200-m depth. Ice coverage was highly variable, and ice floes were generally less than 20 m in diameter and 2.0 m thick. An open region caused a gap in surface track velocity from 2.5 to 6.0 km from the ice edge, making it difficult to calculate wave properties beyond 2 km from the edge. Winds were from the north at  $5\text{ m s}^{-1}$ . Swell of period 11–14 s was observed in ship roll and heave data. Mission 321 on 22 March was completely under ice at 100-m depth. It will only be discussed in relation to wave period, which was observed from the ship to be 12–13 s.

### 3. Analytical methods

#### a. Data processing and results

During mission 324, 25 March 2003, the horizontal velocity of the ice was oscillating, and the magnitude of this oscillation decayed with distance from the ice edge both on the inward and outward segments (Fig. 3). Ice floes were surging and heaving with the surface swell. For the observed range of periods (8–15 s), the deep

water wave speed is much larger than the vehicle speed ( $13\text{--}23\text{ m s}^{-1}$  as compared with  $1.6\text{ m s}^{-1}$ ), and wavelength (100–350 m) is much greater than floe size ( $<20\text{ m}$ ). In this regime, the ice floes nearly follow the circular path of a point on the water surface. Meylan and Squire (1996) calculate that for waves of 100-m wavelength and floes of 50-m diameter and 1 m thick, the surge response is 70% of wave amplitude. As floes become smaller and waves become longer, as in this case, the response approaches 100%. Therefore, the surface track velocity is regarded as a measurement of surface wave orbital velocity superposed on mean ice velocity (southeastward in the case of mission 324). It should be noted that the vehicle depth (greater than 90 m) was greater than the depth of significant wave orbital velocity for 8–15-s waves, so vehicle motion was not influenced by the surface wave field. At periods of 16–26 s, the vehicle surge due to horizontal wave orbital velocity (up to  $0.10\text{--}0.20\text{ m s}^{-1}$ ) may contaminate the measurement of horizontal ice velocity. Vehicle surge response is low, much lower than the heave response due to the aerodynamic shape of the vehicle. Also note vehicle heave plays very little role in the measurement of horizontal ice velocity. The exponential decay of wave orbital velocity with depth has been examined with the subsurface ADCP data in order to confirm the magnitude of the surface orbital velocity. The velocity profiles have a sidelobe layer that is nearly as deep or deeper than the depth of the deepest observable orbital velocity, so it would be dubious to extrapolate the tail of the exponential to the surface. However, if the mean is removed from each bin in mission 321 for under-ice data, the theoretical vertical profile of orbital velocity for a surface wave of 12 s and 1.5 m is consistent with the zero-mean ADCP data, even in the sidelobe layers.

To analyze the complex-valued surface velocity the series is divided into a number of approximately stationary blocks, each lasting 512 s (or about 800 m). (See inset of Fig. 3.) Next the directional wave spectrum is calculated for each segment. By forming the corresponding scalar wave spectrum at set intervals from the ice edge, any trend in significant wave height, mean, and peak wave periods as well as any change in the energy of various wave components can be detected. Since the directional wave spectrum is calculated in this work, wave direction and spread as a function of frequency are also available for each interval.

The directional wave spectrum,  $E(k, \theta)$ , can be separated into a simple frequency-dependent wave spectrum,  $S_{\eta\eta}(f)$ , and a directional distribution,  $D(f, \theta)$ :

$$E(k, \theta) = S_{\eta\eta}(f)D(f, \theta). \quad (1)$$

The wave spectrum is defined as the spectral density function whose integral equals the variance of the sea surface height. Since the integral of the directional spectrum must also equal the same variance, the integral of the directional distribution must be unity for a given frequency:

$$\int_0^{2\pi} D(f, \theta) d\theta = 1 \quad \text{for all } f \geq 0. \quad (2)$$

The directional distribution will be discussed later, but for now,  $S_{\eta\eta}(f)$  must be computed from the series of horizontal wave orbital velocity measurements. To do this, the relationship between sea surface height and velocity of that surface is used. For a deep-water surface gravity wave traveling in the  $x$  direction with amplitude  $A$ , wavenumber  $k$ , and angular frequency  $\omega$ , the orbital velocity of a particle at depth  $z$  is

$$\begin{aligned} U_{\text{orbital}}(x, z, t) &= [\omega \exp(-kz)]A \sin(kx - \omega t) \\ &= \omega \exp(-kz)\eta(x, t). \end{aligned} \quad (3)$$

Of course, (3) holds for a single wave component, but an analogous relationship holds for a sum of linear wave components, which approximates the sea surface. Simply put, the variance in sea surface height of a wave field is proportional to the variance in wave orbital velocity at that location. Furthermore, the spectral density of the sea surface height variation at a given frequency,  $f$ , is proportional to the spectral density of the horizontal orbital velocity at the same frequency:

$$S_{\eta\eta}(f) = [2\pi f \exp(-kz)]^{-2} S_{uu}(f). \quad (4)$$

The proportionality factor is the deep water wave value for the transfer function used in the PUV (P: Pressure, U: eastward velocity, V: northward velocity) method of wave measurement (e.g., Gordon and Lohrmann 2002). Using this factor, measurements of horizontal velocity are used to calculate the wave spectrum. The wavenumber  $k$  must be written in terms of linear frequency  $f$  using the dispersion relation  $\omega = 2\pi f = (gk)^{0.5}$ . If the wave dispersion relation were different (such as in pancake ice), then appropriate forms of (3) and (4) must be used. See LeBlond and Mysak (1978, chapter 11) for a more general expression of (3) for open water. Since we have allowed an infinite number of wave components traveling in different directions, the horizontal wave orbital speed  $U$  is a complex variable. It is equal to  $u + iv$ , where  $u$  is the detrended eastward velocity and  $v$  is the detrended northward velocity.

The scalar spectrum of complex velocity over each 512-s block (256 data points) from the ice edge is calculated using a multitaper method with  $NW = 6$  and six eigenspectra (Percival and Walden 1993, chapter 7).

The spectrum is then transformed using (4). The observed wave spectra for the forward motion of the vehicle are then corrected using the transformation outlined in Wadhams (1978):

$$f_s - f = 2\pi g^{-1} V f^2 \cos(\psi) \quad \text{and} \quad (5)$$

$$S_{\eta\eta}(f) = [1 - 4\pi g^{-1} V f \cos(\psi)] S_{\eta\eta_s}(f_s). \quad (6)$$

Here  $f_s$  and  $S_{\eta\eta_s}$  are the sampled frequency and wave spectrum, respectively;  $V$  is the speed of the vehicle, and  $\psi$  is the angle of the vehicle heading relative to the wave group heading. It is assumed that the wave directional distribution,  $D(\omega, \theta)$ , has a single, identical peak direction at all frequencies. [The calculation of  $D(\omega, \theta)$  is described below.] The transformation corrects for vehicle speed. The vehicle was beyond the depth of significant wave motion, so platform surge is not considered. However, it is necessary to consider the ‘‘spectrum of encounter’’ of the waves observed from the moving platform. For example, in the early part of mission 324, as the vehicle entered the ice pack, the waves were following the vehicle. Therefore, the spectral energy was actually at a slightly higher frequency than observed. The shape was also modified by the factor in (6), which ranges from 1 at low frequencies to about 0.5 at the highest observed frequencies. Any backscattered waves will be incorrectly shifted, as noted by Wadhams (1978). This is a potential (and intractable) problem with waves encountering ice floes. He also notes that explicitly accounting for the directional distribution has been found to give very similar results to assuming a single direction. Of course, if there are two identifiable wave groups traveling in vastly different directions, one cannot apply the same transformation to both. Fortunately, such a situation is not encountered here. For mission 324, as in other missions, surface gravity wave energy is especially strong from 0.06 to 0.1 Hz (Fig. 4). Wave energy at all observed frequencies decreases rapidly with distance into the ice pack. The spectral levels below 0.045 Hz have been set to zero because the transfer function in (4) becomes infinite near the origin and artificially inflates the spectrum at low frequencies. For mission 324 the angle  $\psi$  was less than  $30^\circ$ .

Still following Wadhams (1978), the transformed wave spectra are used to calculate the attenuation rate of wave energy with distance from the ice edge. The attenuation rate depends on frequency: the spectral energy around 0.1 Hz falls more than two orders of magnitude over 7 km, while the energy around 0.06 Hz falls roughly one order of magnitude (Fig. 4). Seven frequency bins are formed. The bin centers are separated by one bandwidth (approximately 0.025 Hz) so that the mean value of the spectral estimate in a given bin is

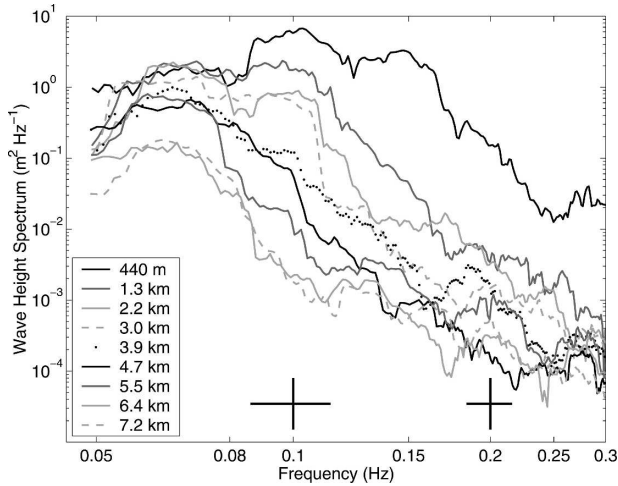


FIG. 4. Wave height spectra for Autosub mission 324, inward series. Each line represents one 512-s segment of ice velocity data centered at the distance from the ice edge given in the legend. Ice velocity spectra have been transformed to wave height spectra, then corrected for Autosub speed and heading. See text. The 95% confidence intervals and bandwidths for two frequencies are indicated by crosses. Spectral levels below 0.045 Hz are set to zero.

independent of the other bins. For each frequency bin a mean spectral density as a function of distance from the ice edge is computed (Fig. 5). The attenuation rate  $\alpha$  of wave energy is defined by

$$S_{\eta\eta}(f, x) = S_{\eta\eta}(f, 0) \exp(-\alpha x) \quad (7)$$

and can be found by plotting the logarithm of spectral density versus linear distance and calculating the slope. The slope of the line is found by applying a linear best-fit model. Note that the best fit is applied to spectra corrected for observer motion using (5) and (6). Distance from the ice edge for each 512-s block of observations is corrected as follows. If the vehicle (roughly traveling perpendicular to the ice edge) encountered waves traveling in a different direction, then, assuming those waves came from the open ocean, they traveled farther to arrive at that location than did the vehicle. Therefore, the  $x$  used in (7) is  $x_v \sec(\psi)$ , where  $x_v$  is the vehicle's distance from the ice edge. It should be noted that some earlier work includes an additional factor in the expression for  $x$ , which is the mean ice concentration over the path. Spectral values deemed to be below the noise floor of the spectral estimates have been left out of the slope calculation. Higher frequencies generally have larger negative slopes and therefore are more strongly attenuated. The attenuation rates themselves will be discussed later.

The 1D wave spectrum can be used to calculate mean wave period and significant wave height. The standard

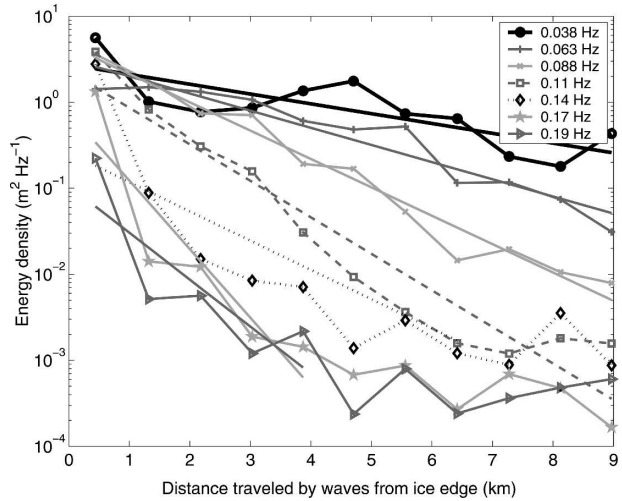


FIG. 5. Attenuation of wave energy in seven frequency bins as a function of distance traveled by the wave group for mission 324 on the way into the ice pack. Linear best-fit lines are based on data points above the noise floor of the spectral estimate, in this case  $1 \times 10^{-3} \text{ m}^2 \text{ Hz}^{-1}$ . The 0.038-Hz lines have been raised two orders of magnitude in order to show clearly the various trends. Attenuation calculations for waves of this low frequency are compromised by possible surge response of the vehicle.

definitions are given in terms of spectral moments (see Anttil et al. 1993, and references therein):

$$m_j = \int_0^{f_c} f^j S_{\eta\eta}(f) df. \quad (8)$$

The Nyquist frequency is  $f_c$ . Note that the order-zero spectral moment is simply the variance of the sea surface displacement. The significant wave height is simply related to the zeroth spectral moment:

$$H_{m0} = 4m_0^{0.5}, \quad (9)$$

and the mean period is defined as

$$T_{m02} = \left( \frac{m_0}{m_2} \right)^{0.5}. \quad (10)$$

Missions 322–324 contain suitable under-ice data from which mean period and significant wave height are computed approximately every 800 m (Fig. 6). Data collected upon entering and exiting the ice pack are treated independently. Mean period was typically from 10 to 15 s. All five series reveal increasing period with distance from the ice edge in the first 6 km. On only two occasions did Autosub travel more than 6 km from the ice edge, and the trends of period with distance oppose each other in these cases. In all cases significant wave height showed rapid decay from 2–3 m at the ice edge to values  $<1$  m several kilometers inward from the edge.

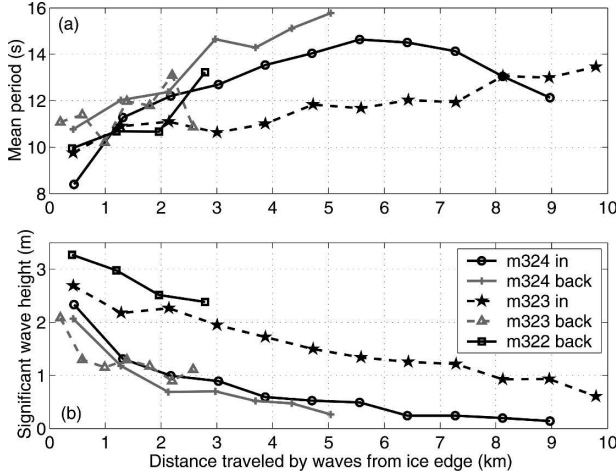


FIG. 6. (a) Mean wave period and (b) significant wave height for Autosub missions 322–324. The label “in” refers to the series collected upon entering the ice pack, while “back” refers to the return series. Period and wave height are derived from the one-dimensional wave spectrum of 512-s blocks (with the exception of the mission 323 return trip, which was so short that 256-s blocks were analyzed).

We now return to the directional distribution,  $D(f, \theta)$ , and its computation from the observed complex surface orbital velocity. Typically, directional wave properties are determined from acoustic profilers using the PUV wave analysis method (Gordon and Lohrmann 2002). This method must be modified to compute directional wave properties with only two components of velocity. Of course, because the wave pressure (or equivalently sea surface height) is not known, the ambiguity in wave direction implied by surface velocity alone cannot be resolved. For example, at a given time, the horizontal velocity is maximum and positive. This could mean the measurement was collected at a crest and the wave was traveling in the positive direction or the measurement was from a trough for a wave moving in the negative direction. However, useful information on mean direction and directional spread of the waves can be collected. The simplest way to calculate the directional distribution is to compute the spectral matrix  $\mathbf{S}$  for each block of data:

$$\mathbf{S} = \begin{bmatrix} S_{uu} & S_{uv} \\ S_{vu} & S_{vv} \end{bmatrix}. \quad (11)$$

Then the spectral matrix in a rotated coordinate system is calculated:

$$\mathbf{S}'(f, \theta) = \mathbf{J}\mathbf{S}\mathbf{J}^T, \quad (12)$$

where the rotation matrix (with  $\theta$  increasing in steps of  $1^\circ$  counterclockwise from the positive  $x$  axis) is

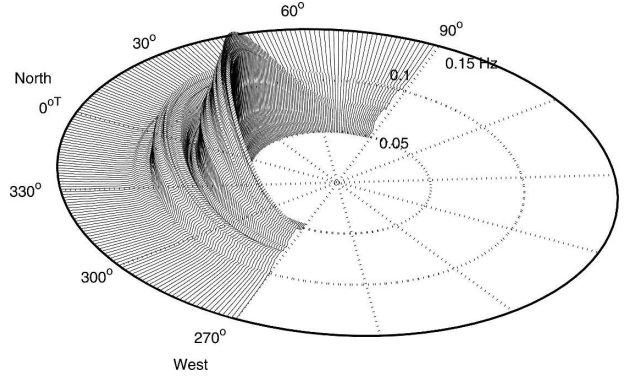


FIG. 7. Directional wave spectrum for the third segment of mission 324 inward series (centered at 2.2 km from the ice edge). The waves were traveling north–south, and peak energy was at a frequency of about 0.06–0.07 Hz.

$$\mathbf{J} = \begin{bmatrix} \cos(\theta) & \sin(\theta) \\ -\sin(\theta) & \cos(\theta) \end{bmatrix}. \quad (13)$$

Next  $\mathbf{S}'(1, 1)$  is normalized for each frequency by dividing by its sum over all angles. The result is the directional distribution  $D(f, \theta)$ . To compute the full directional wave spectrum  $E(f, \theta)$ , (1) is used. In words, for a given frequency, the simple one-dimensional wave height spectrum is distributed among directions according to the distribution calculated by rotating the spectral matrix. For example, if the directional distribution has a single peak direction and does not change much with different wave frequencies (all frequencies traveling in the same direction), then the directional spectrum would simply be a “smeared out” version of the wave height spectrum, with the wave spread determined by the width of the directional distribution. An example directional wave spectrum in Fig. 7 shows how the wave height spectrum, in mission 324, 2.2 km from the ice edge (Fig. 4) is distributed directionally. At all frequencies the waves were traveling north–south with some spread. This is typical, but not always the case: occasionally it is observed that some off-peak frequencies were traveling in different directions, but usually these frequencies are very low in energy. One exception is near the ice edge. In mission 324 three separate wave groups are visible in the wave height spectrum centered at 440 m from the edge (Fig. 8). The primary wave group from Fig. 7 (from 0.06 to 0.07 Hz) is barely visible on the vertical scale of Fig. 8, but it was also traveling north–south. The highest energy wave group at this point near the ice edge was also traveling north–south, but at a higher-frequency range of about 0.09–0.11 Hz. A third wave group was traveling east–west at frequencies between 0.1 and 0.15 Hz. Such directional

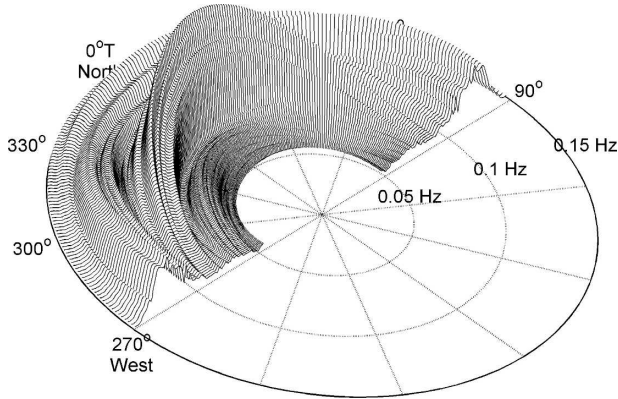


FIG. 8. Directional wave spectrum for the first segment of mission 324 inward series (centered at 440 m from the ice edge). The highest-energy wave group was traveling north–south, and peak energy was at a frequency of about 0.09–0.11 Hz. A secondary wave group was traveling east–west at frequencies between 0.1 and 0.15 Hz. Another secondary wave group from 0.06 to 0.07 Hz, barely visible here, was also traveling north–south (as in Fig. 7). The vertical scale here is different from that in Fig. 7.

spectra for each segment of data are calculated and the mean direction and directional spread of each is examined.

To calculate the mean direction and directional spread, first must be calculated the Fourier coefficients of the directional distribution. The Fourier series representing the directional distribution at each frequency is

$$D(\theta) = \frac{1}{\pi} \left\{ 1 + 2 \sum_{n=1}^{\infty} [a_n \cos(2n\theta) + b_n \sin(2n\theta)] \right\}, \quad (14)$$

where

$$a_n = \int_0^{\pi} D(\theta) \cos(2n\theta) d\theta \quad \text{and} \quad (15)$$

$$b_n = \int_0^{\pi} D(\theta) \sin(2n\theta) d\theta \quad (16)$$

for  $n = 1, 2, 3$ .

Note that  $D(\theta)$  has a period of  $\pi$ , whereas in the literature (Ancitil et al. 1993; Longuet-Higgins et al. 1963)  $D(\theta)$  has a period of  $2\pi$ . This is a result of the inability to resolve the ambiguity in wave direction using only  $U$  and  $V$ . (The rotated spectral matrix repeats after 0.5 rotation.) Therefore, the Fourier expansion and definition of mean direction are slightly different from the typical ones:

$$\bar{\theta} = \frac{1}{2} \tan^{-1}(b_1, a_1). \quad (17)$$

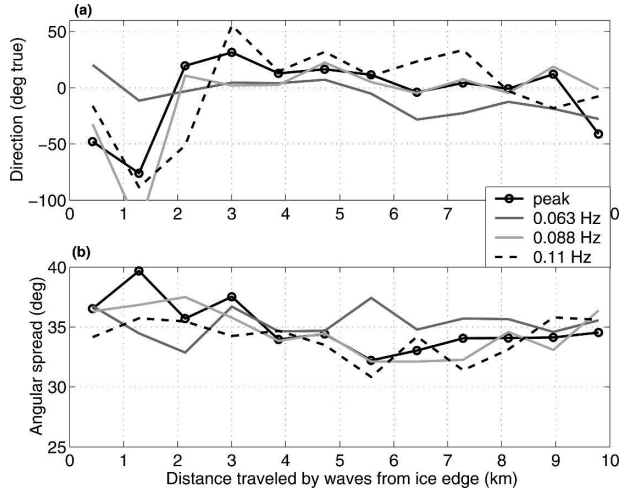


FIG. 9. (a) Mean direction of wave travel and (b) directional spread around that mean for three frequency bins and the peak frequency for mission 323, inward leg. The first 2 km showed higher-frequency waves traveling in directions not perpendicular to ice edge. Further into the ice pack, the direction was fairly steady and nearly perpendicular to the ice edge at all frequencies. The angular spread was fairly steady at all distances from ice edge and all frequencies.

The inverse tangent function in (17) is the four-quadrant inverse tangent with range  $-180^\circ$  to  $+180^\circ$ , which, by itself, represents the mean of  $2\theta$ . The range of (17) is quadrants I and IV. To the directions in quadrant IV,  $180^\circ$  is added to achieve a range of quadrants I and II (allowed due to the directional ambiguity), then angles are converted from geometrical convention to navigational convention. [The positive y axis is  $000^\circ$  T (north) and positive azimuth angles are clockwise.] The procedure was applied to a freely available wave orbital velocity and pressure dataset (<http://www.nortekusa.com/principles/Waves.html>) and compared with the results from the traditional PUV method. Mean direction as a function of frequency is nearly identical for the two methods.

In a similar way, Fourier coefficients are used to calculate the second moment of the directional distribution as a function of frequency, the directional spread:

$$\text{var}[2(\theta - \bar{\theta})] = 2 \int_0^{\pi} \{1 - \cos[2(\theta - \bar{\theta})]\} D(\theta) d\theta \quad (18)$$

and

$$\text{spread} = \text{std}(\theta - \bar{\theta}) = 0.5 \{ \text{var}[2(\theta - \bar{\theta})] \}^{0.5}. \quad (19)$$

Both missions 323 and 324 showed large variations in wave direction near the ice edge (Figs. 9a and 10a). In the first 2 km, higher frequency components tended to be at large oblique angles to the ice edge (which was approximately east–west). At deeper penetrations, the

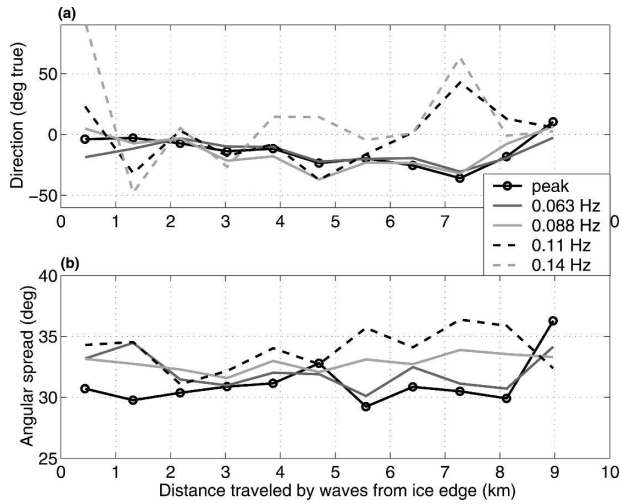


FIG. 10. As in Fig. 9 but for mission 324, inward leg. Many segments showed higher-frequency (off peak) waves traveling in directions not perpendicular to ice edge. Farther into the ice pack and at lower frequencies, the direction was fairly steady and nearly perpendicular to the ice edge. The 0.14-Hz curve is shown for comparison with Fig. 8. Away from the ice edge, energy in this band is negligible. The angular spread was fairly steady at all distances from ice edge, while off-axis wave fields were more divergent.

largest-amplitude waves (those at the peak in the spectra) tended to travel in a direction perpendicular to the ice edge (000° T). Off-peak frequencies were often traveling in different directions, especially for mission 324 (Fig. 10a). Note in Fig. 10a the different directions for the different frequency ranges at the beginning of mission 324, as seen in Fig. 8. There is an indication of wave refraction at the peak frequency for these two missions: the wave direction tends to change with distance into the ice pack; the wave groups veered slightly to the left after they entered the ice pack from the north. The wave spread was remarkably steady, remaining between 30° and 40° for both runs (Figs. 9b and 10b). No trend with distance into the ice pack is present, but the wave groups at the spectral peak tended to be the most tightly focused. During mission 324, higher-frequency wave groups were more spread than lower-frequency wave groups.

*b. Sources of error*

The calculations described above contain assumptions about the time series of horizontal ice velocity. In this section, potential problems with using surface track ADCP measurements in such calculations are considered. First, the ADCP calculates a surface track velocity from the contributions of four components of velocity, one from each acoustic reflection from the surface. Typically these beams are at angle of 20° or 30° from

the normal to the instrument head in both vertical planes: fore-aft and port-starboard. This means that, if the ADCP is pointed vertically upward from a depth of  $H$ , the locations where the beams strike the surface (beam spots) will form the corners of a square. The square will have sides of length

$$2H \tan(\varphi) = 1.16H \quad \text{if } \varphi = 30^\circ \text{ (as in our case).} \quad (20)$$

For the surface track velocity to be considered a point measurement, the size of this square should be much less than the wavelength of the waves being sampled. If it is not, then it is possible, but not necessarily true, that the four velocity components used in the calculation of surface track velocity are out of phase. When the four components are combined, they may partially cancel, resulting in an underestimated velocity magnitude. This calculation is done internally by the ADCP prior to storing the data. During this experiment, the wavelength was typically 150–300 m (10–15-s deep water waves), and vehicle depth was usually 90 m. Therefore, the beam spots formed a square with sides of 104 m, a significant fraction of the wavelength. Clearly, greater vehicle depths exacerbate the problem, and changes in vehicle depth could cause a change in measured surface track velocity magnitude. In addition, changes in heading of the vehicle relative to the wave propagation direction could cause a similar change by changing the relative phases of the four along-beam velocities. Last, vehicle pitch (typically about 3° nose down) changes the beam spot pattern at the surface, and large changes in pitch would change the relative phases of the four components used in the velocity calculation.

Since only the real-time track velocity series is available and not the individual along-beam velocity components, it is not practical to correct the relative phases of the four beam components. Periods where the vehicle depth, heading, and pitch are as steady as possible are chosen, and it is noted that amplitude of the orbital velocity series may be underestimated. In any case, as long as depth, heading (relative to waves), and pitch are steady, the surface track velocity estimate should be consistent. An underestimated velocity would result in an underestimated significant wave height but, if the velocity estimate is consistent, the wave attenuation calculation is correct. The period of the surface track velocity is a robust measurement since all beams measure the same period. (The resulting sum will also have the same, correct period.)

One other issue arises from fact that the surface track velocity is measured with along-beam velocity components. Because the acoustic beams strike the under-ice

surface at an angle, any change in surface slope will cause a change in the along-beam velocity. Consider, for example, a downward-looking ADCP mounted on a vehicle passing over sinusoidal bottom topography of amplitude  $a$ , wavelength  $L$ , with speed  $V$ . Let a single acoustic beam strike the surface at an angle  $\varphi$ . As the acoustic beam scans the sinusoidal surface, the along-beam velocity component will change as the surface approaches and recedes from the vehicle in the direction of the beam. The bottom track velocity will consist of the mean vehicle velocity plus a sinusoidal component of period  $T = LV^{-1}$ :

$$U_{bt}(x) = V + \frac{2\pi a V \tan(\varphi)}{L} \cos\left(\frac{2\pi x}{L}\right), \quad \text{where } x = Vt. \quad (21)$$

The second term arises directly from the fact that the sinusoidal surface gives rise to an along-beam velocity. If the surface slope,  $aL^{-1}$ , is small, this effect is negligible.

In our case, the upward-looking ADCP is scanning an approximately sinusoidal surface (the wave form) that is moving at the wave speed. (The much slower vehicle speed is ignored here.) As a result, the amplitude of the surface track velocity (real ice surging) is modified. For a stationary observer the expected orbital velocity at the surface for the deep water wave is exactly the same as (21) except for the tangent factor. For the ADCP used here  $\varphi = 30^\circ$ . This means that the measured orbital velocity could be too large or too small by a factor of  $\tan\varphi$ , or 58%, independent of wave parameters. However, the orbital velocity is  $90^\circ$  out of phase with this pseudovelocity: the maxima in orbital velocity occur at peaks and troughs, while the maxima due to surface slope occur at the zero crossings. Therefore, the amplitude of the measured orbital velocity [the sum of the true and pseudovelocities:  $\sin(t) + 0.58 \cos(t)$ ] could be too high by 16%. In addition, the four acoustic beams are likely to be measuring different phases of the surface curvature and will tend to cancel, further reducing the 16% error. It is important to note again that the period is a robust measurement. For a stationary observer the period in (21) is identical to the wave period. The amplitude of the surface track velocity is not corrected, but consistency of the surface track velocity measurement is gained by using periods where the depth, pitch, and relative heading were as steady as possible. Thus, the effect of surface slope should be steady, and wave attenuation calculations correct. Wave orbital velocity, however, contains some unknown, but systematic, error up to 16% in magnitude.

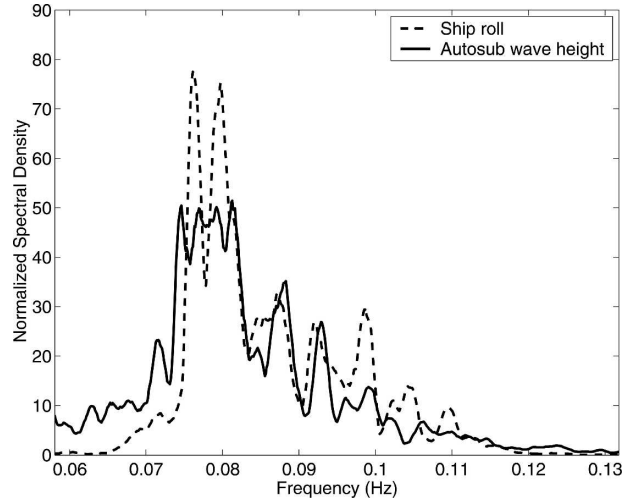


FIG. 11. Wave height spectrum from mission 321 on 22 Mar 2003 (solid). Autosub was 100 m below sea ice. Spectrum of ship roll for the same period of 1.2 h (dashed). Ship was in open water less than 1 km away. Both spectra have been normalized for comparison, both have identical bandwidth ( $0.0028 \text{ s}^{-1}$ ), and both have been smoothed with a 10-point moving average. Note the broad peak between 0.075 and 0.085 Hz (12–13 s).

This type of error can only lead to an overestimate of the true wave orbital velocity.

## 4. Discussion

### a. Scalar wave properties

The wave periods derived from Autosub's upward-looking ADCP compare well with wave periods estimated from ship records of heave and roll. In the case of mission 321, the vehicle and the ship were less than one kilometer apart. The wave orbital velocity under the ice for the entire 1.2-h run is converted to a wave height spectrum as described above (Fig. 11). The normalized spectrum of ship roll for the same period contains the same peak from 0.75 to 0.85 Hz (12–13 s). The spectra also have similar shape outside the peak area. Autosub observations of wave period and spectral shape are thus independently validated, being in excellent agreement with nearby ship observations. Validation of absolute spectral levels (e.g., wave height) and wave directional properties are not possible quantitatively. However, the spectral levels (in particular the rate at which wave energy in various frequency bands decays) and the directional properties can be compared to previous experiments as well as to qualitative expectations based on theory.

Waves of shorter periods are generally attenuated more strongly, although there is a suggestion of “roll-over” near 8–9 s (Fig. 12). At periods shorter than the

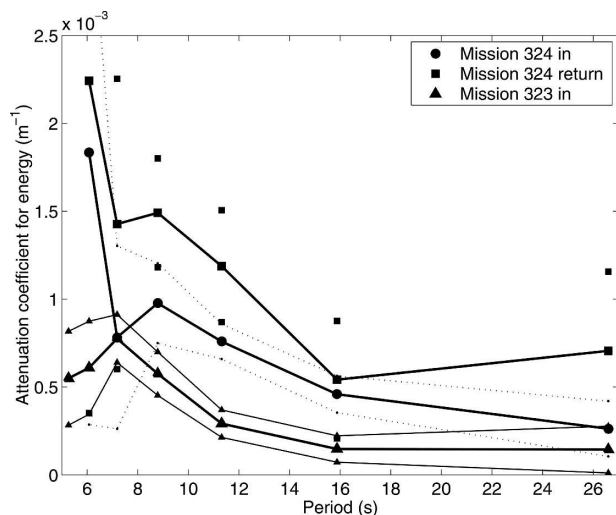


FIG. 12. Energy attenuation coefficient as a function of wave period. Autosub mission 324 indicates increasing attenuation at shorter periods, while mission 323 (triangles) indicates a rollover in attenuation at about 7 s. Confidence levels of 95% are shown by the small symbols with thin lines and are based on the deviations from the best-fit lines, as in Fig. 5. Attenuation values for waves of period longer than 16 s are compromised by possible surge response of the vehicle.

rollover period, attenuation drops slightly. Unfortunately the error in fitting the best line at these short periods is quite large, except for mission 323. The trend of increasing attenuation at shorter periods has been observed many times (Wadhams 1973, 1975, 1978; Wadhams et al. 1986, 1988) and is predicted by several models (Wadhams 1973, 1986; Weber 1987; Liu and Mollo-Christensen 1988; Liu et al. 1991). Other studies have observed (Wadhams et al. 1988) or predicted (Liu et al. 1991) the rollover in attenuation to be between 5 and 10 s. While the general behavior of wave attenuation as a function of frequency fits previous observations qualitatively, floe size distribution, ice coverage, and ice thickness strongly affect the attenuation of waves in sea ice, and there is not sufficient information about them to quantitatively compare the present observations with a model prediction. It is possible, however, to compare with observations in similar ice conditions, as follows.

Wadhams (1986) reports wave attenuation by a field of small floes in Antarctic pack ice from C. H. Dean. The attenuation coefficient for wave energy calculated from 0.5 to 2.0 km from the ice edge was  $8 \times 10^{-4} \text{ m}^{-1}$  at 9 s, which increased to a peak at  $1.5 \times 10^{-3} \text{ m}^{-1}$  at 7 s, then decreased to  $4.5 \times 10^{-4} \text{ m}^{-1}$  at 6 s. These data fall within our range of values. Liu et al. (1991) collected attenuation data from the Labrador Ice Margin Experiment on 25 March 1987 using ice motion pack-

ages at 0.5, 1.5, 2.8, and 4.3 km from the ice edge. As in the present study, ice floes were less than 20 m in diameter and about 1.5 m thick. Liu et al. observed similar attenuation rates of  $2.5 \times 10^{-4} \text{ m}^{-1}$  at 16 s, increasing to  $1 \times 10^{-3} \text{ m}^{-1}$  at 10 s and  $1.6 \times 10^{-3} \text{ m}^{-1}$  at 7.5 s. They did not observe the “rollover” effect but, as in our case, error bars were large at short periods.

In other studies, the observed period generally increased with distance into the ice pack, consistent with our observations. In Liu et al. (1991), wave periods were 8.7–10 s near the edge and 8.7, 9.5, and 18.0 s at 1.5, 2.8, and 4.3 km, respectively. This trend is expected since the shorter-period waves are attenuated more rapidly. The shift of the peak in the wave spectrum to longer periods for waves traveling through an ice field is predicted by Meylan et al. (1997).

### b. Directional wave properties

Our observations indicate changes in the direction of the primary wave group over the first 10 km of sea ice. Using SAR, Larouche and Cariou (1992) also observed wave refraction, which was ascribed to observed inhomogeneities in the ice field (concentration or floe size) and/or current shear. Unfortunately no detailed spatial observations of the ice field along the vehicle track were collected. However, horizontal variations in near-surface water velocity are available from the subsurface bins of the vehicle’s ADCP. The currents at maximum profile range from the vehicle (depths of 40–50 m when the vehicle was at 90 m) show no evidence of horizontal shear, nor does the surface track velocity show a trend in mean velocity (Fig. 3). Wadhams et al. (1986) observed no changes in mean direction based on two stations positioned either side of an ice band less than 1.2 km apart. Wave direction is not predicted to change by current models, such as that of Meylan et al. (1997), since the models assume a uniform ice field over an irrotational fluid (no horizontal shear).

In missions 323 and 324, the wave spread remained steady between  $30^\circ$  and  $35^\circ$  over 10 km. In contrast, the 12–13 July 1984 Greenland Sea experiment (Wadhams et al. 1986) reported a large wave spread of  $60^\circ$ – $80^\circ$  at 17-km and 22-km penetration as compared with only  $42^\circ$  at a point 8 km outside the ice edge. Meylan et al. (1997) predicted that the observed 12–13 July 1984 open sea spectrum should retain its open-sea value of spread even up to 22 km into the ice pack, a result that is more consistent with observations of wave spread reported in this paper. The 13–14 July results of Wadhams et al. (1986) were in better agreement with the theory: 7-s waves were spread slightly (from  $29^\circ$  to  $32^\circ$ ) in the first 1.2 km of pack ice, in good agreement with the predictions of Meylan et al. (1997) ( $29^\circ$ – $36^\circ$ ).

Broadening in directional spread is dependent upon period, ice thickness, and floe diameter (Meylan et al. 1997). While peak wave period in the Greenland Sea study (about 10 s) was similar to this study, ice conditions were different: floes were from 70 to 350 m across and 3 m thick. However, the ice conditions in the present study were similar to a simulation of Meylan et al. (1997), where wave spread increased very little in 10 km for a 10-s sea traveling into a field of 50-m-wide floes 1 m thick. Ice concentration was 50% in the simulation. During missions 323 and 324, floes were roughly 20 m in diameter, and concentration was 80%–100%. The directional spectra in Figs. 7 and 8 are strikingly similar to Meylan et al. (1997), with the exception that both incoming and backscattered waves are combined onto the half circle because of the directional ambiguity. Small changes in the incoming wave spread may be undetectable because of the superposition of the more isotropic backscattered waves on the directional spectra.

## 5. Conclusions

To our knowledge, these are the first scalar and directional wave data collected by an AUV under sea ice, as well as the most complete field study of directional spectra in sea ice. A technique for processing ADCP horizontal velocity to estimate scalar and directional wave parameters has been developed. With proper deployment, this technique can be used with an ordinary ADCP to collect directional wave spectra, both under ice and in open water. In cases where one needs information on waves at various locations, one can use an AUV-mounted ADCP in standard mode to characterize the deep water wave field from depths below the wave influence. After data collection, wave period, direction, and directional spread can be calculated along the vehicle track. In this way, AUVs carrying out dedicated science missions for other purposes can be thought of as “AUVs of opportunity” regarding wave information.

We find that the exponential attenuation of waves propagating through sea ice depends on period in a way that agrees qualitatively with previous observational and numerical experiments. Mean period increases with distance from the ice edge due to selective damping of high-frequency waves, as expected from previous work. Waves appear to have been refracted, which has been observed previously in at least one case, but not in others. In this case it is not clear by what mechanism the waves were refracted, but it is likely to have been inhomogeneities in the ice field, for example, floe size or concentration. Unfortunately, detailed observations of such properties do not exist. Wave spread does not

seem to relate to distance from the ice edge, contrary to some observations. However, wave spreading is sensitive to wave period and ice conditions, in particular floe diameter. Model predictions of wave spreading for wave and ice conditions similar to the present study are very small, and would not be evident in the data presented here. Directional spectra are very similar to those of the numerical simulations of Meylan et al. (1997). More under-ice runs are needed to confirm these observations. Numerical modeling would benefit from an attempt to reproduce these observations, although observations of ice conditions here are somewhat limited. Ultimately, improved models of the propagation of waves in sea ice could imply significant changes to the predicted evolution of the MIZ. Wave attenuation may give rise to enhanced ice–ocean exchanges, which would result in a thinner, weaker ice cover near the ice edge. With improved models, it may be possible to use wave attenuation observations to infer ice properties, such as mean floe size or thickness, along wave group trajectories.

*Acknowledgments.* We thank the Autosub team of National Oceanography Centre, Southampton, the captain and crew of the British Antarctic Survey's *James Clark Ross*, Chris Banks of the Open University (for sea ice observations), and Mark Brandon of the Open University (for data on winds and ship motion). We also thank Peter Wadhams and one anonymous reviewer for their helpful remarks. This work was supported by the U.K. Natural Environment Research Council (Grant NER/T/S/2000/0987) as part of the Autosub Under Ice thematic program.

## REFERENCES

- Ancil, F., M. A. Donelan, G. Z. Forristall, K. E. Steele, and Y. Ouellet, 1993: Deep-water field-evaluation of the NDBC-SWADE 3-M discus directional buoy. *J. Atmos. Oceanic Technol.*, **10**, 97–112.
- Brumley, B., B. Strong, and E. Terray, 2003: Can wave direction be measured from an AUV? *Proc. IEEE/OES Seventh Working Conf. on Current Measurement Technology*, San Diego, CA, IEEE, 140–144.
- De Leonibus, P. S., 1963: Power spectra of surface wave heights estimated by measurements made from a submerged hovering submarine. *Ocean Wave Spectra: Proceedings of a Conference*, Prentice Hall, 243–249.
- Earle, M. D., L. E. Borgman, and T. R. Mettlach, 2002: Ocean surface wave measurements using a small autonomous underwater vehicle. *Proc. Oceans '02 MTS/IEEE Conf.*, Biloxi, MS, IEEE, 272–276.
- Gordon, L., and A. Lohrmann, 2002: Near-shore Doppler current meter wave spectra. *Proc. Fourth International Symp. on Wave Measurement and Analysis: WAVES 2001*, San Francisco, CA, ASCE, 33–43.
- Larouche, P., and C. Cariou, 1992: Directional wave spectra esti-

- mation in a marginal ice zone using linear prediction. *J. Phys. Oceanogr.*, **22**, 196–206.
- LeBlond, P. H., and L. A. Mysak, 1978: *Waves in the Ocean*. Elsevier, 602 pp.
- Liu, A. K., and E. Mollo-Christensen, 1988: Wave propagation in solid ice pack. *J. Phys. Oceanogr.*, **18**, 1702–1712.
- , B. Holt, and P. W. Vachon, 1991: Wave propagation in the marginal ice zone: Model predictions and comparisons with buoy and synthetic aperture radar data. *J. Geophys. Res.*, **96**, 4605–4621.
- Longuet-Higgins, M. S., D. E. Cartwright, and N. D. Smith, 1963: Observations of the directional spectrum of sea waves using the motions of a floating buoy. *Ocean Wave Spectra: Proceedings of a Conference*, Prentice Hall, 111–136.
- Macovsky, M. L., and G. Mechlin, 1963: A proposed technique for obtaining directional wave spectra by an array of inverted fathometers. *Ocean Wave Spectra: Proceedings of a Conference*, Prentice Hall, 235–241.
- Meylan, M. H., and V. A. Squire, 1996: Response of a circular ice floe to ocean waves. *J. Geophys. Res.*, **101**, 8869–8884.
- , —, and C. Fox, 1997: Toward realism in modeling ocean wave behavior in marginal ice zones. *J. Geophys. Res.*, **102**, 22 981–22 991.
- Millard, N. W., and Coauthors, 1998: Versatile autonomous submersibles—The realisation and testing of a practical vehicle. *Underwater Technol.*, **23**, 7–17.
- Percival, D. B., and A. T. Walden, 1993: *Spectral Analysis for Physical Applications: Multitaper and Conventional Univariate Techniques*. Cambridge University Press, 583 pp.
- Squire, V. A., J. P. Dugan, P. Wadhams, P. J. Rottier, and A. K. Liu, 1995: Of ocean waves and sea ice. *Annu. Rev. Fluid Mech.*, **27**, 115–168.
- Terray, E. A., R. L. Gordon, and B. H. Brumley, 1997: Measuring wave height and direction using upward-looking ADCPs. *Proc. Oceans '97 MTS/IEEE Conf.*, Halifax, NS, Canada, IEEE, 287–290.
- , B. H. Brumley, and B. Strong, 1999: Measuring waves and currents with an upward-looking ADCP. *Proc. IEEE Sixth Working Conf. on Current Measurement*, San Diego, CA, IEEE, 66–71.
- Wadhams, P., 1973: The effect of a sea ice cover on ocean surface waves. Ph.D. dissertation, University of Cambridge, 223 pp.
- , 1975: Airborne laser profiling of swell in an open ice field. *J. Geophys. Res.*, **80**, 4520–4528.
- , 1978: Wave decay in the marginal ice zone measured from a submarine. *Deep-Sea Res.*, **25**, 23–40.
- , 1986: The seasonal ice zone. *The Geophysics of Sea Ice*, N. Untersteiner, Ed., Plenum, 825–991.
- , V. A. Squire, J. A. Ewing, and R. W. Pascal, 1986: The effect of the marginal ice zone on the directional wave spectrum of the ocean. *J. Phys. Oceanogr.*, **16**, 358–376.
- , —, D. J. Goodman, A. M. Cowan, and S. C. Moore, 1988: The attenuation rates of ocean waves in the marginal ice zone. *J. Geophys. Res.*, **93**, 6799–6818.
- , F. Parmiggiani, and G. de Carolis, 2002: The use of SAR to measure ocean wave dispersion in frazil-pancake icefields. *J. Phys. Oceanogr.*, **32**, 1721–1746.
- , —, —, D. Desiderio, and M. J. Doble, 2004: SAR imaging of wave dispersion in Antarctic pancake ice and its use in measuring ice thickness. *Geophys. Res. Lett.*, **31**, L15305, doi:10.1029/2004GL020340.
- Weber, J. E., 1987: Wave attenuation and wave drift in the marginal ice zone. *J. Phys. Oceanogr.*, **17**, 2351–2361.